APPLIED SCIENCES AND ENGINEERING

Design of nondeterministic architected structures via bioinspired distributed agents

Jiakun Liu†, Xiaoheng Zhu†, Walker Gosrich, Mark Yim, Jordan R. Raney*

Nature manufactures structures via decentralized processes involving groups of agents. This is fundamentally different from traditional manufacturing, where objects are produced via sequences of predefined steps. In this work, we explore the idea of using simulated "swarms" of simple agents to generate new designs for architected materials in a decentralized, bioinspired manner. Individual agents choose their own actions based solely on information in their immediate environment, with no centralized control. The structures that these processes produce are the result of the collective action of the individual agents, rather than a predetermined design. We build an integrated platform for determining "rule-structure-property" relationships, analogous to process-structure-property relationships in materials science. The platform simulates agent behaviors to show how different rules and different environments result in different structures. We then three-dimensional print these and perform finite element analysis to experimentally and numerically characterize mechanical properties, including tensile strength and energy dissipation.

INTRODUCTION

Materials in nature often exhibit a notable degree of spatial variation and/or stochasticity in structural hierarchy across different length scales. These qualitative differences result from the different manufacturing processes used in the two cases: Synthetic structures are typically designed and built using deterministic processes, in which a target set of geometric and compositional features are precisely defined and, subsequently, translated into a serial list of manufacturing instructions [e.g., for machining or three-dimensional (3D) printing]. In contrast, natural materials are generated by decentralized, distributed processes involving many simple agents. For example, honeycombs are generated via the collective action of many bees, each of which performs actions based on its local environment rather than on a high-level, deterministic plan (*1*, *2*). Termite nests are also constructed via distributed action, with spontaneous organization via stigmergic communication (*3*). Taking inspiration from termite mounds, swarms of robots have also been used to build structures with simple rules running on each robot (*4*). Likewise, the collective action of many cells produces tissues in the body. This is typical of biological manufacturing processes: They build nuanced, multiscale structures via the collective behavior of many simple, distributed agents (bees, cells, etc.) that manipulate their environment based on local cues. The agents individually make use of local information (e.g., gradients in chemistry and moisture) rather than a global, deterministic plan.

Advanced manufacturing techniques (including 3D printing) follow the deterministic workflow of traditional manufacturing: All structural and compositional features must be determined in advance; an ordered list of precise steps must be followed; and, often, the material feedstock must be pure and homogeneous. While these techniques can enable extreme precision, the processes are brittle: Material defects, interfacial incompatibilities, and process deviations may cause immediate failure or unexpected premature failure when the structure is mechanically loaded. Moreover, these processes are often only able to manipulate structural features at one length scale. In contrast, it is recognized that nature is able to optimize for multiple seemingly contradictory properties simultaneously [e.g., strength and toughness; (*5*)] precisely because of the control of specific material hierarchies at multiple length scales (*6*–*8*).

In recent years, researchers have begun to consider the use of swarms of robots to cooperatively build structures [e.g., (*9*, *10*)]. These robotic agents can realize decentralized robot behavioral adaption (*10*–*12*).

In parallel, advances in microrobotics have enabled construction of a large number of microrobotics with increasing hardware capabilities (*13*–*15*). Robots or groups of robots have demonstrated material deposition in a variety of past work including robots depositing expanding structural foam (*16*, *17*) and depositing concrete (*18*, *19*). In each of these cases, the robots are either teams of robots or individual units that could easily be a component of a swarm. Based on these and other advances, a future can be envisioned in which microrobotic swarms could enable new bioinspired, nondeterministic manufacturing approaches, with many simple agents collectively building structures via simple decisions in response to their local environment, with the potential advantage of generating bioinspired, hierarchical structures, and/or structures that are fine-tuned to their local environment.

One challenge with these approaches, however, is that such decentralized, distributed assembly results in stochastic features. There have been numerous previous studies on understanding how different periodic structural features lead to different mechanical properties (i.e., structure-property relationships), including those based on struts (*20*–*23*), plates (*24*, *25*), and shells (*26*, *27*).

However, periodic lattices may not be optimal in heterogeneous environments (e.g., when a part must be designed to interface with other irregular parts or when the environment itself is irregular). Recently, there has been a growing interest in understanding the effect of stochasticity in the design of such structures and their structure-property relationships (*28*–*31*), as stochasticity can be beneficial for certain properties, such as resistance to mechanical failure. For example, many researchers have analyzed mechanical and/or failure behavior of nonperiodic, disordered, or imperfect lattice structures

Department of Mechanical Engineering and Applied Mechanics, University of Pennsylvania, Philadelphia, PA 19104, USA.
*Corresponding author. Email: raney@seas.upenn.edu
†These authors contributed equally to this work.

by introducing structural variations/stochasticity into perfect lattices (*32*–*35*). Recent work has shown how structures can be designed via a stochastic growth process in which each constitutive cell (building block) of the structure can be assigned a random choice from a predefined set of patterns (with restrictions associated with structural integrity) (*29*, *31*). As another example, researchers have demonstrated the use of a data-driven framework with a large number of compositional microstructures with various morphological descriptors to study the structure-property relationships of disordered networks (*30*).

Here, we generate nondeterministic architected materials via simulations of swarms of simple, distributed bioinspired agents. We start by considering simple rules that agents might obey and the structures that would result from these distributed rules (analogous to process-structure relationships in materials science). Then, we quantify the mechanical properties (e.g., strength and energy dissipation) of the structures generated by these rules (analogous to structure-property relationships in materials science). We subsequently consider how different assumptions about the capabilities of the agents, such as additional sensing modalities, would enable additional behaviors (and, hence, different structures and properties). Our approach is conceptually different from existing approaches, with the nondeterministic structural features intrinsically generated via the collective action of a large number of simple, decentralized agents (which are only aware of their immediate environment), rather than assuming a limited set of preexisting structural motifs and/or using algorithms to perturb or introduce disorder/randomness in topology (*29*, *30*, *35*).

RESULTS

Rule-structure-property relationships of distributed agents

Rules for distributed agents

Here, we develop a 2D framework for simulating how swarms of agents subjected to different local rules, parameters, and hardware assumptions would generate different types of structures. We assume the agents are capable of a few simple, elemental behaviors (basic functions):

1. Motion: Agents are able to move but may be subjected to movement limitations.

2. Material deposition: Each agent is capable of depositing material as it moves but may be limited by the amount of material it can deposit.

3. Sensing the environment: Agents are assumed to be able to sense their local environment, specifically whether there is already material in their local environment. The size of this sensing area and the type of signals that the agents can sense can be parameterized. The area that an agent can sense from a given position is referred to as the agent's "view."

In this work, we focus solely on rules that generate lattice structures, i.e., nodes connected by straight edges. Of course, rules can be as complex as desired. However, the more complicated the rule, the more complex the hypothetical agents would need to be to implement it (e.g., processing power and available sensing modalities). Even simple rules can generate a large variety of nondeterministic structures via different parameter combinations.

For example, agents could move solely via "random walk" while extruding material and one would find that a wide variety of nondeterministic structures could be generated, depending on the specific parameters that are chosen. Figure S1 (A and B) shows that a simple change in the amount of material that the agents are allowed to produce (using a random walk movement strategy and fixing all other parameters) can lead to qualitatively different structural features, with the generated structures varying from sparse, chain-like architectures to dense, foam-like architectures. As another example, fig. S1 (C and D) shows structures generated with the same parameters as in fig. S1A, but with the agents only allowed to enter the area from the bottom border. The resultant structures exhibit noticeable direction-dependent topological features. The rest of the study will specifically focus on rule-structure-property relationships related to architected lattices (i.e., nodes connected by edges).

n-Furcation

Using the basic functions introduced above as a foundation, we implemented an "*n*-Furcation" rule (i.e., a generalization of bifurcation and trifurcation). It has the advantage of remaining relatively simple (i.e., containing only three basic function), yet is capable of generating notable structural variations. This rule is inspired by collective construction procedures in nature (e.g., bees constructing honeycombs) (*2*, *3*) and also by recursive biostructure formation processes [e.g., development of vascular networks or trabecular bones; (*36*)].

The *n*-Furcation rule is implemented as follows (Fig. 1):

1) We first define a construction space (size limit of the lattice) to be 40 mm by 40 mm. In each simulation, one agent first enters the construction area and randomly deposits an initial strut. Once the first strut has been deposited, the first agent leaves the construction space. Then, the remaining agents enter into the construction space.

2) As a new agent moves into the construction space, it starts to search for existing struts. If an agent senses an existing strut, then it turns and moves toward it. Once it reaches the strut, it turns to move along the strut, choosing the direction randomly. If the agent has not spotted any strut and has reached the boundary of the construction space allowed by the simulation, it leaves the construction space (i.e., it no longer participates in the simulation).

3) Once an agent reaches the end of a strut, it rotates by the turning angle $\pm\theta_i$ and moves along the next strut, if there is one, or starts to deposit a new strut for a targeted distance L_i if no strut is detected.

4) During deposition of a new strut, an agent continues to monitor the local environment. The agent will stop depositing the current strut once a strut length of L_i has been achieved or the strut being deposited makes contact with an existing strut before reaching a length L_i. Once an agent has stopped its material deposition (whether completed as originally planned or terminated), it leaves the construction space along its current direction.

5) The amount of deposited material (quantified as the total length of all struts) is tracked in each numerical step. Structure generation terminates when the total length of the struts remains unchanged for a prolonged duration of 10^4 consecutive steps. For comparison, an agent typically remains in the deposition space for fewer than 200 steps.

6) In the later stage of the construction process, the agents tend to traverse existing struts instead of reaching empty or incomplete regions in the inner domain. To improve the overall deposition efficiency, we added a parameter representing the probability (typically, 50%) that an agent would skip a strut. This creates a better spatial distribution of agents later in the process.

In this work, our goal is to use the simplest possible rules to generate versatile lattice structures with tunable stochasticity and tunable properties. From past work on cellular mechanics, it is known

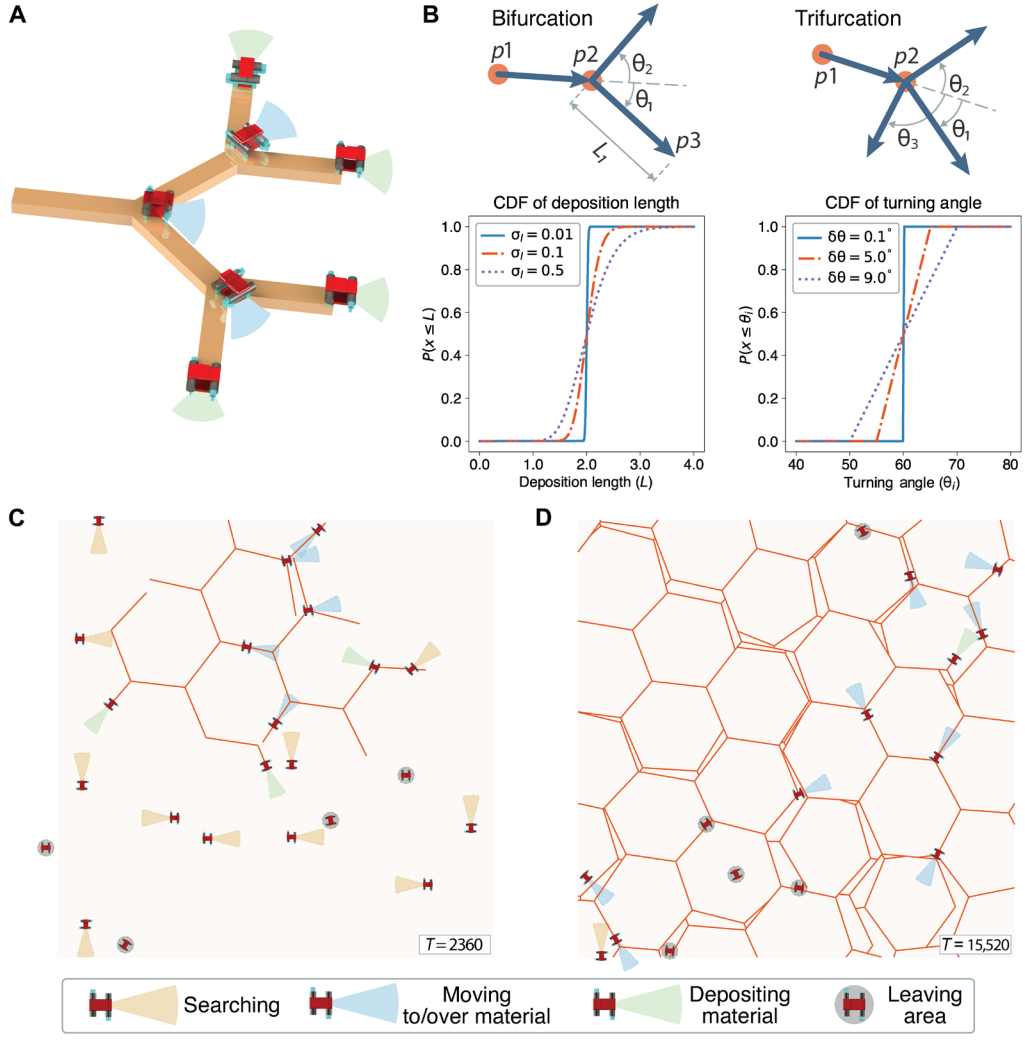

Fig. 1. *n*-Furcation rule for agent behavior. (**A**) Schematic showing agents and associated material deposition. (**B**) Definition of *n*-Furcation for the special cases of $n = 2$ (bifurcation) and $n = 3$ (trifurcation). The plots show the cumulative distribution function of L_i and θ_i given different deviation values, with $L^* = 2$ and $\theta_i^* = 60°$, respectively. (**C** and **D**) Two snapshots of the simulated agents and associated deposited materials while the agents are implementing a bifurcation rule (i.e., $n = 2$) with parameters ($L^* = 5$ mm, $\delta\theta = 5°$, and $\sigma_l = 0.05$), showing early and late stages (with time labeled at bottom right) of the simulation, respectively. The legend at the bottom describes the status of the agents, where the color of an agent's view specifies the type of its active task, and a gray circle (replacing its view) indicates the agent is leaving the construction space, i.e., not actively viewing its surroundings.

that the strut length L and lattice angle θ_i are two essential parameters for defining the structure and properties of lattices (*37*, *38*). The turning angle, θ_i, is determined by the number of possible branches an agent can follow when it reaches the end of a strut (i.e., reaches a node). For example, hexagonal structures are defined by a coordination number of three (i.e., three struts meet at each node). Hence, to ensure hexagonal symmetry, an agent that is moving along a strut could branch in one of the two different directions when it reaches a node. This corresponds to an *n*-Furcation branching parameter of $n = 2$ (denoted as "bifurcation"). This is shown schematically in Fig. 1A.

We also allow probabilities to be assigned to the agents' behaviors, resulting in statistical variation (Fig. 1B). These variations can be used to account for intrinsic errors/uncertainty in hardware. For example, the real turning angle θ_i is decided by the targeted turning angle θ_i^* and hardware intrinsic error $\delta\theta$.

The probability density function (PDF) of the real turning angle, θ_i, can be expressed as

$$\text{PDF of } \theta_i: \quad f(\theta_i) = \begin{cases} \dfrac{1}{2\delta\theta}, & \text{for} \quad \theta \in [\theta_i^* - \delta\theta; \theta_i^* + \delta\theta] \\ 0, & \text{for} \quad \theta \notin [\theta_i^* - \delta\theta; \theta_i^* + \delta\theta] \end{cases} \tag{1}$$

Similar to the turning angle, the material deposition length L_i is assumed to follow a normal distribution with a mean value of L^* (the targeted deposition length) and deviation of σ_l. The PDF and cumulative distribution function (CDF) of the actual deposition length, L_i, can be expressed as

$$\text{PDF:} \quad f(L_i) = \frac{1}{L_i \sigma_l \sqrt{2\pi}} \exp\left\{ -\frac{1}{2} \left[\frac{\ln(L_i) - \ln(L^*)}{\sigma_l} \right]^2 \right\} \tag{2A}$$

$$\text{CDF:}\quad F(L_i)=\frac{1}{2}\left\{1+\text{erf}\left[\frac{\ln(L_i)-\ln(L^*)}{\sqrt{2}\sigma_l}\right]\right\} \tag{2B}$$

Characterization of rule-structure relationships

Following the above definitions, we simulated the bifurcation ($n = 2$) rule for a wide range of parameters to understand their effects on the generated structures. The essential parameters for the simulations are listed in Table 1. The parameters that are varied in the parametric study are marked in bold. The ranges over which the parameters are varied are shown in brackets. Figure 1 (C and D) shows two snapshots from the same simulation, at earlier and later time steps, respectively. The parameters used in this particular simulation were $L^* = 5$ mm, $\delta\theta = 5°$, and $\sigma_l = 0.05$. An animation showing the behavior of the agents, including their motion and their collective generation of a structure via material deposition, is shown in movie S1. To ensure the correctness of our simulations, we first simulated bifurcation with targeted turning angles of $\theta^*_{i=1,2} = \pm 60°$ with no stochasticity (i.e., σ_l and $\delta\theta$ are both zero). As shown in Fig. 2A, in this case, the agents generate a regular, periodic hexagonal pattern without any statistical deviations or defects. The other plots in Fig. 2, i.e., panels B, C, and D, show structures generated with stochasticity in deposition length (L_i), turning angle (θ_i), or both of these, respectively. Note that the variation in strut lengths in Fig. 2C is not the result of planned variation in deposition lengths. Rather, it is a necessity that arises from variations of the turning angles of the agents.

Although we focused on hexagonal lattices ($\theta^*_{i=1,2} = \pm 60°$), other lattices can be generated with this simulation platform (e.g., square lattices can be generated using $\theta^*_{i=1,2} = \pm 45°$, as shown in fig. S3).

Characterization of structure-property relationships

The mechanical properties of regular structures, including periodic hexagonal lattices like that shown in Fig. 2A), have been studied extensively (*38*). Stochastic structural features are of increasing interest to researchers, as they can be beneficial in certain circumstances, e.g., enhancing failure resistance. Here, we numerically and experimentally characterize the structure-property relationships of the lattices previously generated by the bifurcation rule. The general approach is to translate the lattices generated in the "Characterization of rule-structure relationships" section into models that can be studied both numerically and experimentally.

To do this, we integrated the numerical swarm robotic simulation framework with in-house Abaqus preprocessing scripts. By translating the structures into Abaqus, we were able to conduct simulations to numerically evaluate the mechanical properties of the structures generated by the swarms. The structures generated in Abaqus can also be stored as CAD files for 3D printing, enabling experimental validation of the same structures being numerically characterized. Such an integrated rule-structure-property platform enables rapid design, numerical prediction, and prototyping with experimental validation. We focus on cellular lattice structures with relative densities ranging from 0.1 to 0.3. We are particularly interested in finding structures that simultaneously maximize (i) uniaxial tensile strength and (ii) the amount of energy dissipated by the structure when loaded to ultimate failure. It should be noted that instead of calling this second property "toughness," a material property, we instead refer to it as structural energy dissipation. In this study, the energy dissipation of a lattice specimen is defined as the area under its load-displacement curve obtained via uniaxial tensile loading

Table 1. Parameters for simulations.

	Definition	Parameter	Value/range
Modeling space	Span of construction area in the horizontal *x* axis	Ω_x	40 mm
	Span of construction area in the vertical *y* axis	Ω_y	40 mm
2-Furcation (bifurcation)	Targeted value (mean) of turning angles	$\theta^*_{i=1,2}$	±60°
	Error between actual and targeted turning angle	$\delta\theta$	[0, 5]°
	Targeted value (mean) of deposition length	$\boldsymbol{L^*}$	[1, 6] mm
	Standard deviation of deposition lengths	σ_l	[0,0.3] mm
Agent motion	Default moving speed per numerical time unit	$\boldsymbol{V^a}$	0.05 mm/step
	Speed when depositing material (slow)	$\boldsymbol{V^a_l}$	0.005 mm/step
	Speed when leaving the construction area (fast)	$\boldsymbol{V^a_u}$	0.1 mm/step
Agent size and view	Body dimension (edge length)	$\boldsymbol{D}^{\text{agt}}_{\text{body}}$	0.5 mm
	View distance when in active tasks (not leaving area)	$\boldsymbol{D}^{\text{agt}}_{\text{view}}$	1.5 mm
	View angle (between two edges of its view wedge)	$\theta^{\text{agt}}_{\text{view}}$	30°

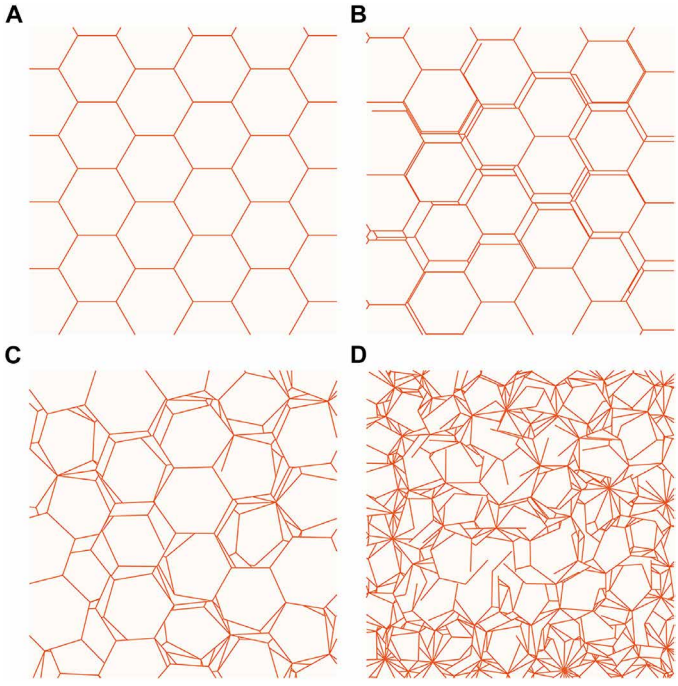

Fig. 2. Structures generated by agent simulations implementing bifurcation. (**A**) If no stochasticity in turning angle (θ_i) or deposition length (L_i) is allowed, i.e., $\delta\theta = 0$ and $\sigma_l = 0$, then a regular hexagonal structure is generated. (**B**) Stochasticity is allowed, but only for the deposition length ($L^* = 5.0$ mm and $\sigma_l = 0.1$ mm). (**C**) Stochasticity is allowed for the turning angle ($\theta = 60°$ and $\delta\theta = 5°$). By necessity, this induces some stochasticity in deposition length (L_i) due to termination of material deposition by agents when encountering existing struts. (**D**) Stochasticity is allowed for both parameters ($L^* = 5.0$ mm, $\sigma_l = 0.3$ mm, $\theta = 60°$, and $\delta\theta = 10°$).

$$U = \int_0^{\Delta} F \, d\Delta \tag{3}$$

To achieve accurate numerical predictions of structural properties and failure behaviors, we developed a user-defined material subroutine (UMAT) on the basis of a series of tensile tests of 3D printed specimens, including conventional load-to-failure tests and cyclic loading tests. More details on the characterization of material properties and constitutive equations are provided in the Supplementary Materials. Next, we validated the UMAT by 3D printing lattice structures that were designed via swarm simulations and experimentally testing these to failure, comparing the mechanical response to the finite element analysis (FEA) results. The overall loading curve, ultimate tensile load, and progressive damage were in close agreement. As an example, Fig. 3 shows a comparison between numerical and experimental results for three structures. Figure 3A shows the crack path predicted numerically (left) and measured experimentally (right) for the three structures. Figure 3B shows a comparison of the experimental and numerical tensile load-displacement relationships, from which the maximum load and total energy dissipation can be extracted (Fig. 3C), showing reasonable agreement. Additional experimental data, characterization of material constitutive laws, and details about the integrated numerical platform are provided in the Supplementary Materials. We also include the FEA/experimental (EXP) comparison of 10 more samples in fig. S4.

After validating the numerical model, we numerically studied the structure-property relationships of a large number of structures with various values of L^*, σ_l, and $\delta\theta$ (i.e., the parameters listed in bold in Table 1). The results are summarized in Fig. 3D, where data points are categorized into four groups on the basis of assigned variations in $\delta\theta$ and/or σ_l (demonstrated by the four examples shown in Fig. 2). We observe that structures with high stochasticity (i.e., those generated with higher statistical variation in key parameters) typically exhibit a larger percentage of energy dissipation after the yield strain is exceeded compared to the regular lattice. This improvement results from the larger ultimate tensile displacement (see Fig. 3D, i and ii, and fig. S5). Representative loading curves of lattices with low/medium/high stochasticity are provided in fig. S5. In general, the disordered structures fail in a stable progressive way, whereas regular lattices break catastrophically once their maximum tensile strength is reached. With increasing stochasticity, architected structures have lower tensile strength but higher fracture strain (see, e.g., fig. S5). With excessive stochasticity, the strength of architected structures is unavoidably degraded, requiring one to choose an appropriate degree of stochasticity for the intended application. The improvement in the ultimate tensile displacement brings benefits for creatures in nature. As biological systems need to be adaptable to various loading and boundary conditions to improve their survivability, an extended ultimate failure displacement may allow a bio-structure to survive and repair itself.

Distributed agents with local interaction

As is evident in Fig. 2 (B and D), the simple agents and rules described in the previous section often result in mechanically inefficient placement of struts (e.g., redundant adjacent struts) that merely increase the mass of the structure without significantly improving its mechanical properties. Here, we consider the use of agents with increased capabilities, i.e., the ability to perform simple communication with nearby agents and to sense additional physical signals, such as temperature.

Definitions of local interactive behaviors

Here, we describe four behaviors that are enabled by the new capabilities of the agents. Note that the agents' actions are still decentralized (i.e., they are not aware of a global plan or non-local information). They merely become capable of improved behaviors with the new ability to adjust their actions in response to information from nearby agents in addition to the local environment. The new behaviors, labeled A to D, are shown schematically in Fig. 4 (A to D) and defined as follows:

1) Rule A (temperature sensing): An agent is capable of sensing temperature and of adjusting its deposition activities in response. For example, here, we assume L^* is inversely proportional to temperature, such that agents tend to deposit shorter and denser struts with increasing temperature (Fig. 4A).

2) Rule B (improved strut alignment): In addition to the basic motion, an agent is allowed to patrol for a short distance (from $p1$ to $p3$) to check its surroundings before it starts its planned material deposition. If the agent detects an existing node ($p4$), then the agent will go back to its initial point $p1$ and adjust its deposition direction to aim at the detected node $p4$. If no node is detected during its patrol, then the agent will go back to point $p1$ and execute its original deposition plan without any adjustment in its direction (Fig. 4B).

3) Rule C (improved strut length): If an agent decides to terminate material deposition at $p1$, then the agent will check if there are

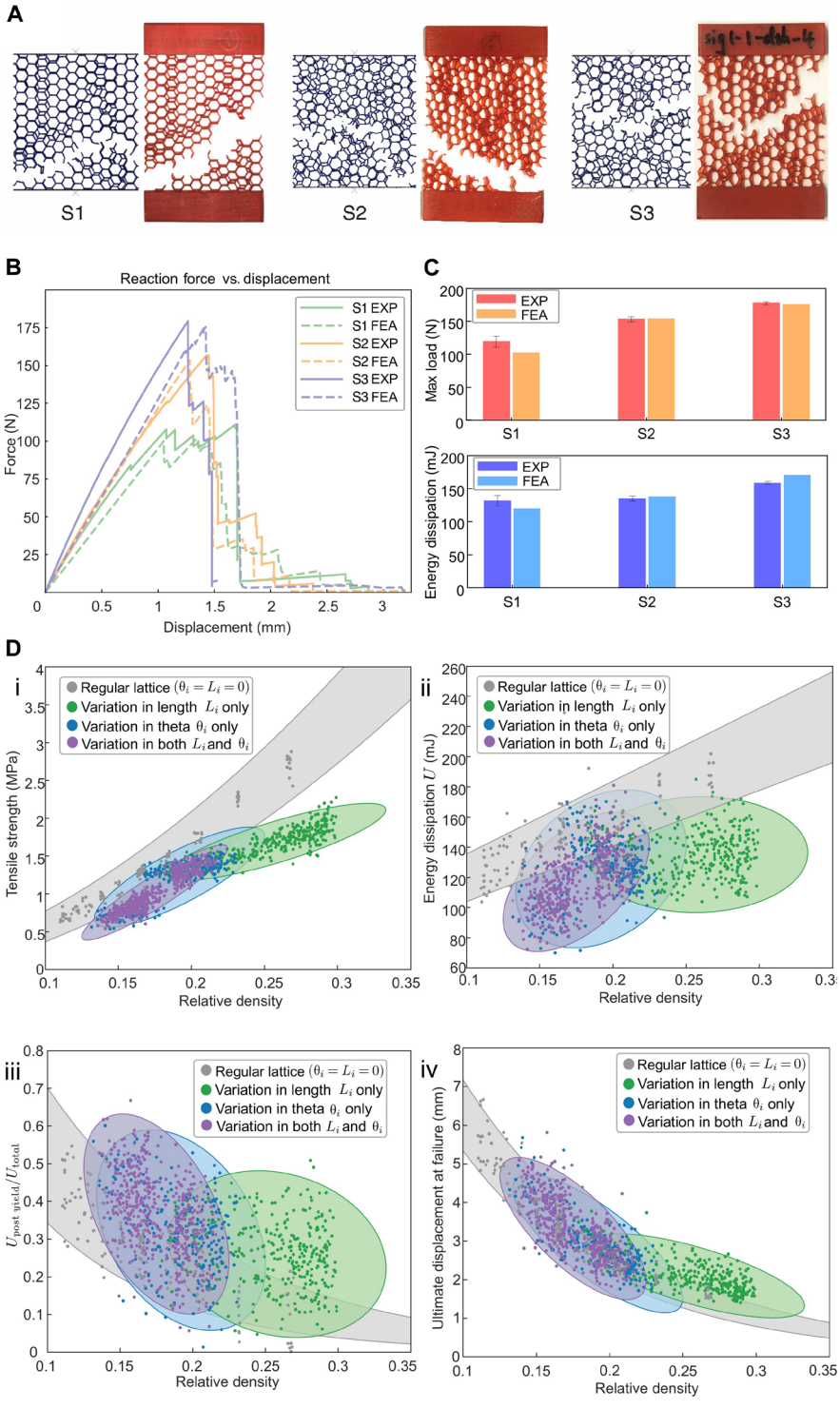

Fig. 3. Comparison of simulations and experiments. (**A**) Comparison of numerical (left) and experimental (right) crack path during failure for three different structures. (**B**) Numerical and experimental load versus displacement measurements for the structures in (A). (**C**) Maximum load and total energy dissipation, extracted from the numerical and experimental load-displacement data in (B). Experimental data are the average of four tests for each structure. (**D**) Scatter plots of 1480 virtual design and tests. Set 1 (shown in gray) represent samples without stochasticity ($\delta\theta = 0$ and $\sigma_l = 0$). Sets 2, 3, and 4 (shown in blue, green, and purple) are structures with stochasticity in turning angles, deposition lengths, and in both, respectively. The ellipses are 95% confidence ellipses (*40*). (i) Tensile yield strength versus relative density. (ii) Energy dissipation versus relative density. (iii) Percentage of energy dissipation after the yield strength ($U_{post\ yield}/U_{total}$) versus relative density. (iv) Ultimate displacement at failure versus relative density.

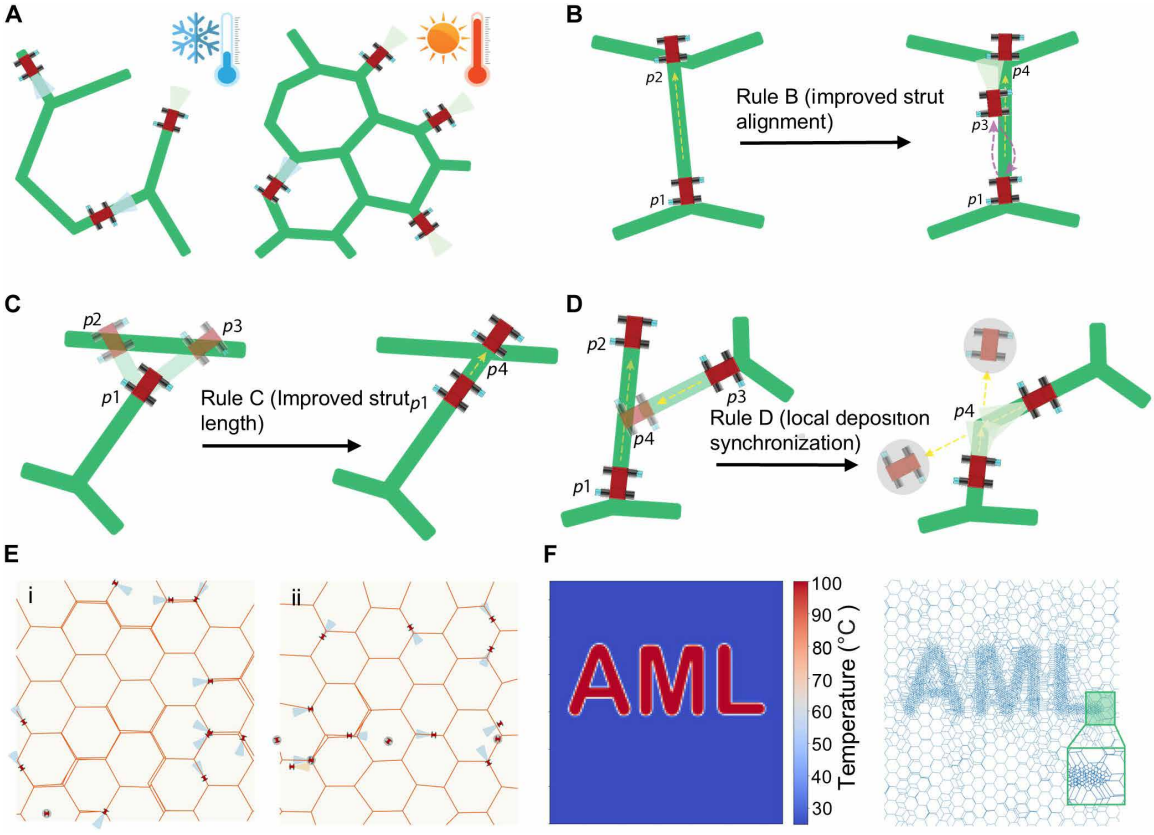

Fig. 4. Local interactive behavior and environmental awareness of agents. (**A**) An agent is able to sense temperature and adjust its deposition activities accordingly. Here, an agent deposits shorter struts when it detects higher temperature. (**B**) An agent can patrol for a short distance along its planned deposition path to check its surroundings and can adjust its angle to align with an existing node near its planned deposition path. (**C**) An agent can extend its initial deposition plan to fill small gaps between its deposited strut and an existing strut. (**D**) An agent can communicate with other nearby agents to complete a node collaboratively. In figures (B) to (D), left sub-picture shows the scenario that would occur without such a function. (**E**) A comparison showing the effect of local interactive behaviors on the generated structures. (i) A structure constructed with small statistical variations in $\delta\theta$ and σ_l, resulting in redundant struts that almost overlap with each other. (ii) A structure generated by agents with extra interactive functions B, C, and D, exhibiting apparent improvement in material allocation efficiency. (**F**) By embedding a high temperature zone representing English letters "AML" (abbreviation of Architected Materials Laboratory), distributed agents with activate function A (temperature awareness) can construct a lattice structure showing the corresponding letters.

any existing struts within its view. If so, the agent will overwrite the termination decision and continue depositing to fill the remaining gap between $p1$ and $p4$ (Fig. 4C).

4) Rule D (local deposition synchronization): An agent can communicate with other nearby agents. If a depositing agent detects another depositing agent on its planned path, then it sends a pairing request to the other agent. Subsequently, the two paired agents will adjust their speed and collaboratively make a common node at $p4$. Without this interactive behavior, the agent would complete its own deposition plan (from $p1$ to $p2$), while the other agent would later encounter this strut and stop its deposition at point $p4$ (Fig. 4D). It is possible that two agents may encounter one another during the construction of a new strut. When an agent encounters another agent, it ceases any ongoing deposition and exits the design space. In contrast, with local interactive functions, two agents that encounter one another may pair with each other to form a single strut or to avoid overlapping deposition paths.

Although the hardware for microrobotic swarms for distributed manufacturing has not yet been realized, behaviors analogous to the local interactive functions of this section have been demonstrated in centimeter-scale robots (*11*, *12*). For example, phototactic robots have shown the capability of collectively nucleating a construction site and cooperatively building organized structures (*11*). Function A is analogous to this work. As another example, robot ants (RAnt) have been demonstrated with the capability of boundary/obstacle detection (*12*). Functions B and C are analogous, enabling agents to change their deposition decisions based on existing boundaries/structures. In the cited work, these RAnts can also interactively escape a trap by collectively moving obstacles away. Function D is analogous, enabling the agents to locally communicate with other agents while depositing materials. We also added a function of skipping existing struts to improve the overall deposition efficiency, similar to the trap-escaping behavior of these centimeter scale robots. Figure 4Ei shows a structure designed by using simple bifurcation with small statistical variations in $\delta\theta$ and σ_l. The statistical variations cause redundant struts that almost overlap with each other. In contrast, Fig. 4Eii shows a structure generated by agents with extra interactive functions B, C, and D, resulting in less redundancy of material placement and improved specific mechanical properties. Figure 4F shows a structure generated in an area with varying temperature

with agents following rule A (temperature awareness). A high temperature region in the shape of the letters "AML" (Architected Materials Laboratory) is applied to the environment. As a result, the agents generate shorter struts and higher local relative density in this region, demonstrating the possibility of adjusting structural features in response to the local environment using distributed agents.

Effect of interactive behaviors on structure properties

We next conducted a parameter sweep and a series of numerical simulations to quantify the rule-structure-property relationships for structures designed using agents capable of rules A to D. We picked two groups of structures (as summarized in Fig. 3D) on the basis of rule parameter sets (stochasticity in deposition length only and stochasticity in turning angle only). We generated 50 structures for each set/combination of rule parameters. As a result, each picked group contains 100 structures (50 from simple bifurcation and 50 from simple bifurcation with the same set of parameters plus additional local behaviors B, C, and D). The tensile strength and energy dissipation, as obtained via these simulations, are shown in Fig. 5. We take structures generated with stochasticity in deposition length only (i.e., $\sigma_l = [0, 0.3]$ and $\delta\theta = 0$) as an example.

The implementation of interactive functions A to D can allow design of structures that at roughly 20% lower relative density (e.g., from 0.156 to 0.126) have only 10% less strength (e.g., from 0.72 to 0.65 MPa). Similarly, interactive functions A to D allow design of structures with 20% lower relative density (e.g., from 0.156 to 0.126) that have 6.8% improvement in energy dissipation (e.g., from 96.8 to 103.4 mJ).

Architected structure design in discontinuous construction area

Perhaps one of the greatest strengths of a distributed design approach is its compatibility with complex environmental constraints, where regular lattices would not be optimal. For example in the construction process of honeycombs, bees preemptively change their building behavior in constrained geometries to merge multiple regular lattices together (*1*). Here, we consider the distributed design of lattices in environments with geometric constraints, leading to discontinuities in the stress profile (Fig. 6A). To generate a suitable lattice for these geometric constraints, we first used FEA to get the von Mises stress contour plot of a linear elastic solid with the particular geometric constraints (e.g., Fig. 6A) subjected to uniaxial tension. The internal geometric features produce the expected stress concentrations (Fig. 6B), suggesting that a lattice constrained to this geometry will require additional reinforcement in these areas to avoid catastrophic failure. Next, we treated the stress contour plot as a scalar temperature field to be imposed on the build area during the distributed manufacturing process. Using agents with temperature sensors and subjecting these to this imposed temperature field causes a higher density of struts to be deposited in the areas that would experience stress concentrations. The agents were assigned a thermal-dependent strut length L^* and allowed functions A, C, and D shown in Fig. 4. For comparison, we also generated a regular lattice with the same geometric constraints (Fig. 6C). To do this, agents were assigned an edge length L^* with zero deviation. Fifty-five structures each were generated for both the temperature-sensitive process and the regular lattices.

Figure 6C shows loading curves and the predicted damage path of a regular lattice and an ACD-activated lattice, both with comparable relative densities. For regular lattices, the crack initiates where the stress is concentrated due to the elliptical voids and then propagates as the load increases. For lattices generated by the distributed agents, multiple cracks initiate at different locations, due to the extra reinforcement and more densely distributed materials where the stress would be concentrated by the elliptical voids. The final failure pattern is thus qualitatively different from that in regular lattices. Figure 6D shows tensile strength versus relative density and energy dissipation versus relative density (left and right, respectively) for the two types of lattices. While the tensile strength at a given relative density is statistically similar in both cases, the average energy dissipation of the lattices generated via the thermally sensitive distributed agents is 19.6% higher than that of the regular lattices for a given relative density. This improvement in energy dissipation is attributed to the more evenly distributed global stress profile in the lattices generate by temperature-sensitive agents. Evenly distributed stress fields help the structure to fracture in a stable, progressive manner. Multiple cracks initiating at different locations create larger fracture surfaces (Fig. 6C) and, hence, higher energy dissipation.

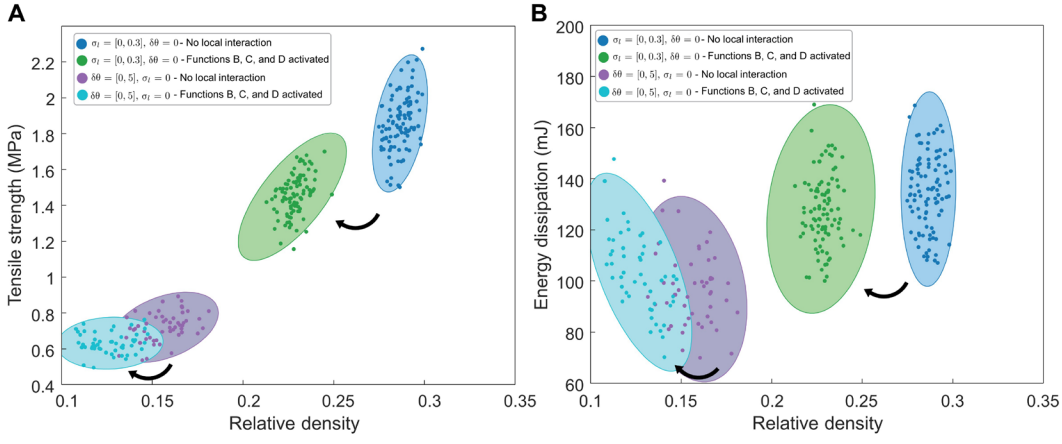

Fig. 5. Comparison between two sets of structures under uniaxial tension to demonstrate effect of local interactive behaviors on the structural properties. In both sets, apparent reduction in relative densities is observed, indicating improved material allocation efficiency. Each set contains 100 samples (50 from simple bifurcation and 50 from simple bifurcation plus local functions). The ellipses are 95% confidence ellipses (*40*) (**A**) Tensile strengths decrease as an inherent result of reduction in relative densities. (**B**) In both sets, the average energy dissipation remains comparable, as the relative density decreases.

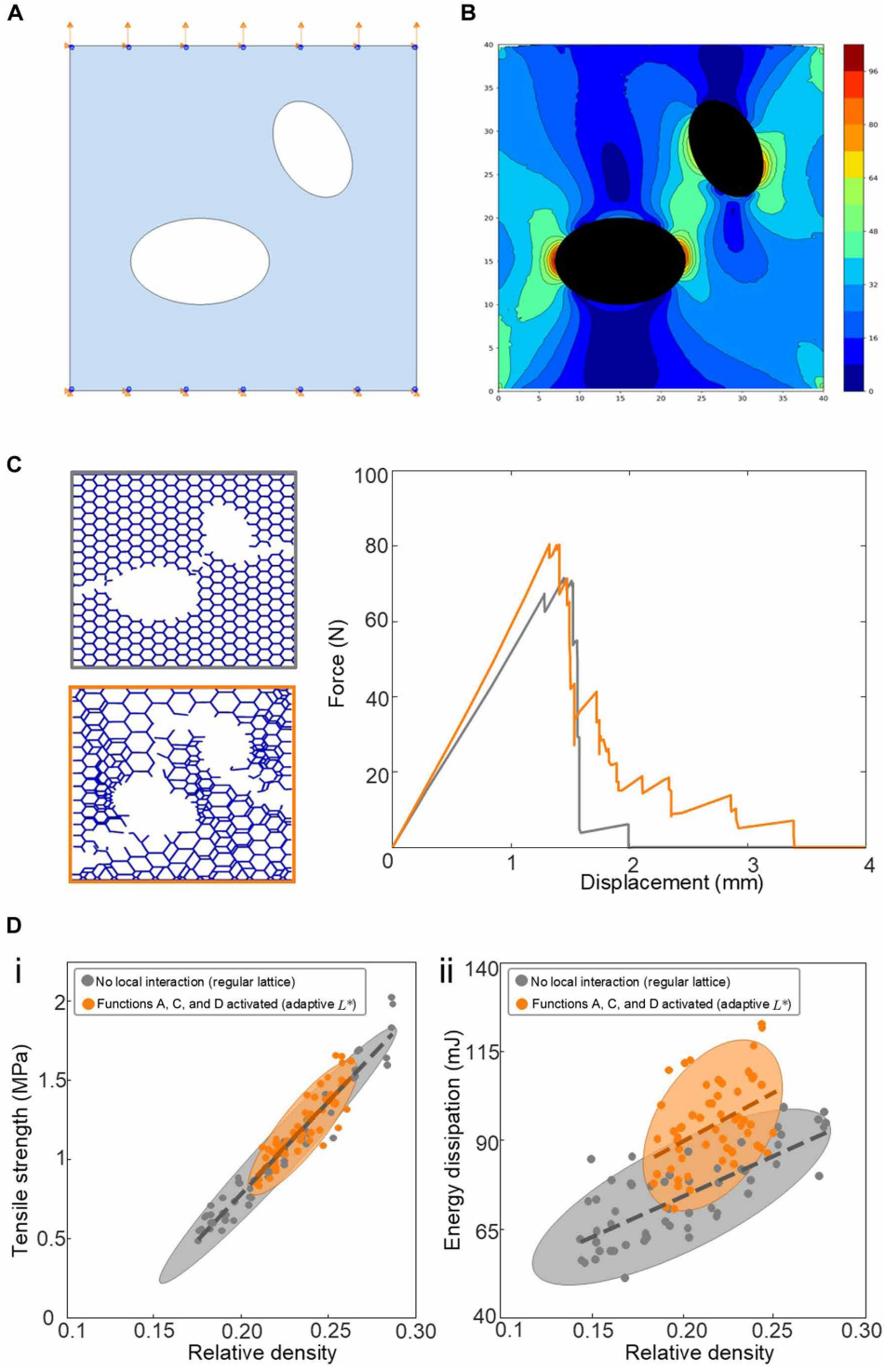

Fig. 6. Structure design example and results. (**A**) Construction area with two elliptical voids. The loading and boundary conditions (uniaxial tension) remain the same as previous examples. (**B**) Temperature field as environmental stimulus for thermally dependent local behavior; the values are proportional to the von Mises stress of a linear elastic solid equivalent to the structure in (A) under tension. (**C**) Predicted damage path with the force-displacement responses for the regular lattices and the lattices generated by temperature-sensing agents, respectively. Due to the extra material deposited around the stress concentrations, the crack paths no longer initiate from the stress concentrated areas as in regular lattices. The two structures shown have comparable relative density (0.204 for regular and 0.199 for disordered). (**D**) (i) Tensile strength versus relative density for both regular lattices and lattices generated by temperature-sensing agents with functions A, C, and D. Dashed lines indicate linear best fit. (ii) Energy dissipation vs relative density for both types of lattices.

DISCUSSION

In this study, we explored the idea of using simulated swarms of simple distributed agents to generate new nondeterministic designs of architected structures. The rules that the agents follow are inspired by manufacturing processes seen in nature, where simple agents, unaware of any global plan, manufacture materials and structures via their collective action. We focused on the *n*-Furcation rule, a general rule for generating lattice structures via the distributed action of agents. We demonstrated a workflow that includes (i) simulating the action of agents (rule-structure relationships), (ii) high-fidelity finite element modeling (e.g., predicting damage evolution), and (iii) rapid prototyping and testing. Through this rule-structure-property platform, we investigated the failure characteristics of agent-generated lattice structures and compared maximum tensile reaction load, total energy dissipation, percentage of energy dissipation post yield strength, and ultimate failure displacement with that of regular lattices.

The assumptions about the agents' capabilities have a large influence on the quality of designs that can be generated. For example, combining capabilities such as temperature-dependent agent activities, detection of local features, and direct interaction/collaboration between agents, can lead to improved distribution of material and thereby to the design of lattice structures with superior mass efficiency (i.e., a given set of mechanical properties can be achieved for lattices with less material). In addition, we also demonstrated the capability of using distributed agents to design architected structures in a discontinuous design space. By activating locally interactive behaviors of agents, architected structures generated by distributed agents exhibit an average improvement of about 19.6% in energy dissipation while maintaining a comparable level of tensile strength relative to regular lattices of comparable relative densities.

In this work, we focused on parameters that generated lattices with relative densities between 0.1 and 0.4, both because this range of relative densities is found in important examples in nature [e.g., honeycomb (*1*), sea sponge (*39*), and ants (*3*)] and because well-known rules for structure-property relationships exist for the mechanical behavior of cellular structures with this range of relative densities. On this basis, we limited the values for targeted deposition length, $L^* \in [1\text{ mm}, 6\text{ mm}]$. Figure S7 shows the typical features of structures generated with deposition lengths significantly larger or smaller than this range. For example, a deposition length of $L^* = 10$ mm results in a small relative density of 0.05 and too few unit cells to model the behavior of the structure as a lattice (fig. S7, left). A deposition length of $L^* = 0.1$ mm results in a large relative density of 0.95, which behaves like a porous material rather than a lattice (fig. S7, right). Despite being primarily numerical, we verified the accuracy of finite element predictions through experimental prototyping and testing. While substantial work on hardware and software is still necessary for manufacturing via distributed agents to become feasible, this work represents an initial step toward the design of robotic agents for swarm manufacturing and introduces a new approach for the nondeterministic design of materials and structures.

MATERIALS AND METHODS

Simulations of structure generation via swarms of agents

Agents are simulated through custom code developed in Python. Location, motion status, and material deposition history of the agents are tracked during the simulations. Deposited materials (struts) are stored by tracking the nodal coordinates of line segments, allowing calculation of termination and intersection points.

Because materials are deposited in the form of struts (straight line segments), vector-based analysis is performed to check whether two line segments are overlapping or colinear. We also performed some pixel-based rule and structure generation but settled on strut-based generation due to easier finite element generation and prototyping (more details on these limitations are provided in the Supplementary Materials). After structures are generated in the swarm simulator, they are passed to the commercial software Abaqus, and custom preprocessing commands (also in Python) are used to (i) generate a 2D finite element model for direct analysis and failure prediction and (ii) generate a 3D model for 3D printing and experimental testing.

Prototyping and experimental tests

All beams in this study have in-plane cross-sectional width of 0.3 mm and out-of-plane thickness of 2.0 mm. For computer-aided design (CAD) models for mechanical tests, extra rectangular regions (Fig. 3) were printed to allow the mechanical test system to grip the specimen. All prototypes for mechanical tests were printed by Digital Light Processing 3D printer EnvisionTEC Vida HD. The printer resolution of the printer is 25 μm, and the span dimension of all lattices (40 mm by 40 mm) is determined considering the size limit of this printer. A photopolymer resin named R11 was used for printing. The resultant samples (after curing) demonstrate elastic behavior, followed by brittle failure. More details involving materials characterization are provided in the Supplementary Materials. The fracture tests of lattices were performed by conducting uniaxial tensile tests under displacement control with a loading rate of 1 mm/min using an Instron-65SC at room temperature.

Finite element analysis

For all simulations, fully integrated 2D continuum shell elements (CPE4 and CPE3) were used. The seed size of mesh was set to 0.15 mm to ensure that there were at least two elements along the cross section of each beam. The mechanical response of R11 was modeled by user defined subroutine (UMAT), and the detailed parameters and equations used for constitutive behavior are provided in the Supplementary Materials.

Supplementary Materials

The PDF file includes:

Supplementary Text
Figs. S1 to S8
Legend for movie S1

Other Supplementary Material for this manuscript includes the following:

Movie S1

REFERENCES AND NOTES

1. M. L. Smith, N. Napp, K. H. Petersen, Imperfect comb construction reveals the architectural abilities of honeybees. *Proc. Natl. Acad. Sci. U.S.A.* **118**, e2103605118 (2021).
2. M. L. Smith, K. J. Loope, B. Chuttong, J. Dobelmann, J. C. Makinson, T. Saga, K. H. Petersen, N. Napp, Honey bees and social wasps reach convergent architectural solutions to nest-building problems. *PLoS Biol.* **21**, e3002211 (2023).
3. A. Heyde, L. Guo, C. Jost, G. Theraulaz, L. Mahadevan, Self-organized biotectonics of termite nests. *Proc. Natl. Acad. Sci. U.S.A.* **118**, e2006985118 (2021).
4. J. Werfel, K. Petersen, R. Nagpal, Designing collective behavior in a termite-inspired robot construction team. *Science* **343**, 754–758 (2014).
5. R. O. Ritchie, The conflicts between strength and toughness. *Nat. Mater.* **10**, 817–822 (2011).

6. R. Lakes, Materials with structural hierarchy. *Nature* **361**, 511–515 (1993).
7. P. Fratzl, Biomimetic materials research: What can we really learn from nature's structural materials? *J. R. Soc. Interface* **4**, 637–642 (2007).
8. B. Gludovatz, F. Walsh, E. A. Zimmermann, S. E. Naleway, R. O. Ritchie, J. J. Kruzic, Multiscale structure and damage tolerance of coconut shells. *J. Mech. Behav. Biomed. Mater.* **76**, 76–84 (2017).
9. K. H. Petersen, N. Napp, R. Stuart-Smith, D. Rus, M. Kovac, A review of collective robotic construction. *Sci. Robot.* **4**, eaau8479 (2019).
10. K. Zhang, P. Chermprayong, F. Xiao, D. Tzoumanikas, B. Dams, S. Kay, B. B. Kocer, A. Burns, L. Orr, C. Choi, D. D. Darekar, W. Li, S. Hirschmann, V. Soana, S. A. Ngah, S. Sareh, A. Choubey, L. Margheri, V. M. Pawar, R. J. Ball, C. Williams, P. Shepherd, S. Leutenegger, R. Stuart-Smith, M. Kovac, Aerial additive manufacturing with multiple autonomous robots. *Nature* **609**, 709–717 (2022).
11. F. Giardina, S. Ganga Prasath, L. Mahadevan, Collective phototactic robotectonics. arXiv:2208.12373 [cs.RO] (2022).
12. S. Ganga Prasath, S. Mandal, F. Giardina, J. Kennedy, V. N. Murthy, L. Mahadevan, Dynamics of cooperative excavation in ant and robot collectives. *eLife* **11**, e79638 (2022).
13. M. Z. Miskin, A. J. Cortese, K. Dorsey, E. P. Esposito, M. F. Reynolds, Q. Liu, M. Cao, D. A. Muller, P. L. McEuen, I. Cohen, Electronically integrated, mass-manufactured, microscopic robots. *Nature* **584**, 557–561 (2020).
14. M. F. Reynolds, A. J. Cortese, Q. Liu, Z. Zheng, W. Wang, S. L. Norris, S. Lee, M. Z. Miskin, A. C. Molnar, I. Cohen, P. L. McEuen, Microscopic robots with onboard digital control. *Sci. Robot.* **7**, eabq2296 (2022).
15. M. Yim, W. Gosrich, M. Miskin, "Buoyancy enabled non-inertial dynamic walking," in *2023 IEEE/RSJ International Conference on Intelligent Robots and Systems (IROS)* (IEEE, 2023), pp. 2665–2672.
16. S. Revzen, M. Bhoite, A. Macasieb, M. Yim, "Structure synthesis on-the-fly in a modular robot," in *2011 IEEE/RSJ International Conference on Intelligent Robots and Systems* (IEEE, 2011), pp. 4797–4802.
17. N. Napp, R. Nagpal, Distributed amorphous ramp construction in unstructured environments. *Robotica* **32**, 279–290 (2014).
18. X. Zhang, M. Li, J. H. Lim, Y. Weng, Y. W. D. Tay, H. Pham, Q.-C. Pham, Large-scale 3D printing by a team of mobile robots. *Autom. Constr.* **95**, 98–106 (2018).
19. S. Joki, P. Novikov, Minibuilders small robots printing large-scale structures (2014); https://iaac.net/project/minibuilders/ [accessed 25 January 2025].
20. R. G. Hutchinson, N. A. Fleck, The structural performance of the periodic truss. *J. Mech. Phys. Solids* **54**, 756–782 (2006).
21. X. Zheng, H. Lee, T. H. Weisgraber, M. Shusteff, J. DeOtte, E. B. Duoss, J. D. Kuntz, M. M. Biener, Q. Ge, J. A. Jackson, S. O. Kucheyev, N. X. Fang, C. M. Spadaccini, Ultralight, ultrastiff mechanical metamaterials. *Science* **344**, 1373–1377 (2014).
22. M. Pham, C. Liu, I. Todd, J. Lertthanasarn, Damage-tolerant architected materials inspired by crystal microstructure. *Nature* **565**, 305–311 (2019).
23. Y. Shao-Yi, S. Lee, Z. Zhang, Z. Jin, X. G. Grace, From brittle to ductile: Symmetry breaking in strut-based architected materials. *ACS Mater. Lett.* **5**, 1288–1294 (2023).
24. Z. Yin, F. Hannard, F. Barthelat, Impact-resistant nacre-like transparent materials. *Science* **364**, 1260–1263 (2019).
25. F. Wang, M. Brøns, O. Sigmund, Non-hierarchical architected materials with extreme stiffness and strength. *Adv. Funct. Mater.* **33**, 2211561 (2023).
26. S. C. Han, J. W. Lee, K. Kang, A new type of low density material: Shellular. *Adv. Mater.* **27**, 5506–5511 (2015).
27. Y. Wang, X. Zhang, Z. Li, H. Gao, X. Li, Achieving the theoretical limit of strength in shell-based carbon nanolattices. *Proc. Natl. Acad. Sci. U.S.A.* **119**, e2119536119 (2022).
28. D. A. van Egmond, B. Yu, S. Choukir, S. Fu, C. V. Singh, G. D. Hibbard, B. D. Hatton, The benefits of structural disorder in natural cellular solids. arXiv:2110.04607 [physics.app-ph] (2021).
29. K. Liu, R. Sun, C. Daraio, Growth rules for irregular architected materials with programmable properties. *Science* **377**, 975–981 (2022).
30. S. Luan, E. Chen, J. John, S. Gaitanaros, A data-driven framework for structure-property correlation in ordered and disordered cellular metamaterials. *Sci. Adv.* **9**, eadi1453 (2023).
31. Y. Jia, K. Liu, X. S. Zhang, Topology optimization of irregular multiscale structures with tunable responses using a virtual growth rule. *Comput. Methods Appl. Mech. Eng.* **425**, 116864 (2024).
32. K. Li, X. L. Gao, J. Wang, Dynamic crushing behavior of honeycomb structures with irregular cell shapes and non-uniform cell wall thickness. *Int. J. Solid Struct.* **44**, 5003–5026 (2007).
33. I. Christodoulou, P. J. Tan, Crack initiation and fracture toughness of random Voronoi honeycombs. *Eng. Fract. Mech.* **104**, 140–161 (2013).
34. H. C. Tankasala, V. S. Deshpande, N. A. Fleck, Tensile response of elastoplastic lattices at finite strain. *J. Mech. Phys. Solids* **109**, 307–330 (2017).
35. K. Karapiperis, D. M. Kochmann, Prediction and control of fracture paths in disordered architected materials using graph neural networks. *Comms. Eng.* **2**, 32 (2023).
36. M. Potente, H. Gerhardt, P. Carmeliet, Basic and therapeutic aspects of angiogenesis. *Cell* **146**, 873–887 (2011).
37. L. J. Gibson, M. F. Ashby, G. S. Schajer, C. I. Robertson, The mechanics of two-dimensional cellular materials. *Proc. R. Soc. Lond. A Math. Phys. Sci.* **382**, 25–42 (1982).
38. L. J. Gibson, M. F. Ashby, *Cellular Solids: Structure and Properties* (Cambridge Solid State Science Series, Cambridge Univ. Press, ed. 2, 2014).
39. M. C. Fernandes, J. Aizenberg, J. C. Weaver, K. Bertoldi, Mechanically robust lattices inspired by deep-sea glass sponges. *Nat. Mater.* **20**, 237–241 (2021).
40. P. Schubert, M. Kirchner, Ellipse area calculations and their applicability in posturography. *Gait Posture* **39**, 518–522 (2014).

Acknowledgments

Funding: We acknowledge the support of the National Science Foundation via grant number 2036881. **Author contributions:** M.Y. and J.R.R. devised the research. All authors designed the research approach. J.L., X.Z., and W.G. performed the research. J.L., X.Z., and J.R.R. wrote the manuscript. All authors edited the manuscript. **Competing interests:** The authors declare that they have no competing interests. **Data and materials availability:** All data needed to evaluate the conclusions in the paper are present in the paper and/or the Supplementary Materials.

Submitted 22 November 2024
Accepted 10 April 2025
Published 14 May 2025
10.1126/sciadv.adu8260